

ARTICLE

Received 17 Sep 2013 | Accepted 22 Nov 2013 | Published 6 Jan 2014

DOI: 10.1038/ncomms4009

OPEN

Structure-based mechanism for Na^+ /melibiose symport by MelB

Abdul S. Ethayathulla¹, Mohammad S. Yousef^{1,†}, Anowarul Amin¹, Gérard Leblanc^{2,†}, H. Ronald Kaback² & Lan Guan¹

The bacterial melibiose permease (MelB) belongs to the glycoside-pentoside-hexuronide:cation symporter family, a part of the major facilitator superfamily (MFS). Structural information regarding glycoside-pentoside-hexuronide:cation symporter family transporters and other Na^+ -coupled permeases within MFS has been lacking, although a wealth of biochemical and biophysical data are available. Here we present the three-dimensional crystal structures of *Salmonella typhimurium* MelB_{St} in two conformations, representing an outward partially occluded and an outward inactive state of MelB_{St}. MelB adopts a typical MFS fold and contains a previously unidentified cation-binding motif. Three conserved acidic residues form a pyramidal-shaped cation-binding site for Na^+ , Li^+ or H^+ , which is in close proximity to the sugar-binding site. Both cosubstrate-binding sites are mainly contributed by the residues from the amino-terminal domain. These two structures and the functional data presented here provide mechanistic insights into Na^+ /melibiose symport. We also postulate a structural foundation for the conformational cycling necessary for transport catalysed by MFS permeases in general.

¹Department of Cell Physiology and Molecular Biophysics, Center for Membrane Protein Research, Texas Tech University Health Sciences Center, Lubbock, Texas 79430, USA. ²Department of Physiology, University of California, Los Angeles, California 90095, USA. † Present addresses: Department of Physics, College of Arts and Sciences, Southern Illinois University, Edwardsville, Illinois 62026-1654, USA (on leave from: Biophysics Department, Faculty of Science, Cairo University, Egypt) (M.S.Y.); CEA-DSV-Fontenay aux Roses, Cross Division of Toxicology, 92 265 Fontenay aux Roses BP 6, France (G.L.). Correspondence and requests for materials should be addressed to L.G. (email: Lan.Guan@ttuhsc.edu).

Membrane transport proteins from the glycoside–pentoside–hexuronide:cation symporter family^{1,2} (TC 2.A.2; Supplementary Fig. S1a,b) are widely found in all life forms, and *Escherichia coli* melibiose permease (MelB_{Ec}) is the best-studied representative. However, our understanding of transport mechanisms with these important permeases is limited by lack of high-resolution structures. *Salmonella typhimurium* MelB (MelB_{St}) has >85% primary sequence identity with MelB_{Ec}^{3,4}, and both proteins exhibit ~54% similarity with the human major facilitator superfamily (MFS) domain-containing protein 2A; moreover, the residues essential for transport in MelB are functionally conserved in MFS domain-containing protein 2A⁵. Remarkably different from other MFS transporters⁶, MelB catalyses electrogenic symport of galactosides with Na⁺, Li⁺ or H⁺ (ref. 7); the broad cation selectivity is a prominent feature. Some MelB orthologues selectively couple sugar symport with one or two out of the three cations, but the anomeric configuration of the sugar is important with respect to specific coupling cations⁷. For instance, sugars in the α -configuration (melibiose and raffinose) utilize all three cations, but β -anomers of galactopyranosides couple only to Na⁺ and Li⁺ (ref. 8).

MelB_{St} shares similarity with regard to cation-coupling specificity and other transport features with the well-studied MelB_{Ec}^{4,7,9–12}. All three coupling cations compete for a single binding site with a protein/sugar/cation stoichiometry of unity^{4,13,14}. Electrogenic sugar symport is driven by $\Delta\tilde{\mu}_{H^+, Na^+ \text{ or } Li^+}$, depending on the coupling cation⁴. Thermodynamically, MelB transduces the free energy from the downhill translocation of a cation to drive translocation of sugar against a concentration gradient and vice versa^{4,12}.

Here we present three-dimensional X-ray crystal structures of MelB_{St} in two distinct conformations, refined to 3.35 Å. The structure is in general agreement with the predicted model of MelB¹⁵. Notably, most MFS members are either H⁺ symporters or uniporters. Among the members with solved structures^{16–23}, MelB_{St} is the sole member that utilizes Na⁺ primarily as a coupling cation for symport and uses a previously uncharacterized coupling mechanism.

Results

Functional characterization. Purified MelB_{St} is monodisperse, stable (Supplementary Fig. S2a,b) and binds melibiose, 2'-(N-dansyl)aminoalkyl-1-thio- β -D-galactopyranoside (D²G) or methyl- β -D-thiogalactoside, but has no affinity for sugars without a galactopyranosyl moiety (Fig. 1a). A single sugar-binding site was determined by isothermal titration calorimetry (ITC; Fig. 1b,c). Melibiose binding is exothermic with a K_d of ~1 mM in the presence of Na⁺ or Li⁺, which is consistent with previous results⁴. Furthermore, sugar binding is driven energetically by a small favourable enthalpy change (ΔH) and a bigger increase in entropy ($T\Delta S$).

Overall fold of MelB_{St}. The structure of MelB_{St} was solved by molecular replacement and refined to a resolution of 3.35 Å (Table 1). The asymmetric unit contains four molecules (Mol-ABCD; Supplementary Fig. S3a,b) with twinning and pseudo-translation symmetries. Surprisingly, twinned Mol-B and Mol-D have a conformation different from Mol-A and Mol-C (Fig. 2 and Supplementary Fig. S4a,b). We describe only Mol-A and Mol-B here as representative structures.

As predicted¹⁵, MelB_{St} adopts a typical MFS fold, organized in amino- and carboxy-terminal six-transmembrane α -helix bundles (Fig. 2), with a connecting cytoplasmic central loop containing two short helices (CH1 and CH2), and the cytoplasmic

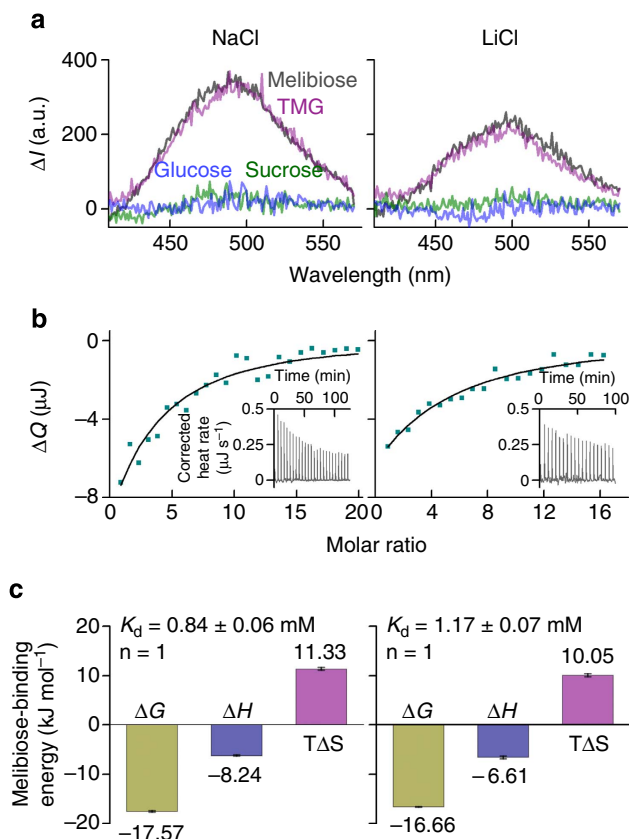


Figure 1 | Functional characterization. Purified MelB_{St} containing 100 mM NaCl or LiCl were subjected to D²G FRET and ITC measurements. **(a)** D²G FRET measurement. With an excitation wavelength of 290, emission spectra were collected between 415 and 575 nm. Difference spectra (ΔI) were calculated before and after addition of a given sugar (50 mM). Grey curves, melibiose; purple curves, methyl- β -D-thiogalactoside (TMG); green curves, sucrose; blue curves, glucose. **(b)** ITC measurement. Melibiose titration thermograms (insets) were recorded at 25 °C. Cumulative heat change (ΔQ) is plotted as a function of the molar ratio of melibiose/MelB_{St}, and fitted with the one-site independent binding model. **(c)** Melibiose-binding energetics. Enthalpy change (ΔH) and the association constant (K_a) were measured directly; dissociation constant $K_d = 1/K_a$; free-energy change $\Delta G = -RT \ln K_a$; entropy change $T\Delta S = \Delta H - \Delta G$; n , stoichiometry. Error bar, s.d., $n = 2$.

C-terminal tail with another short α -helix (CH3). Both the N and C termini are on the cytoplasmic side of the membrane and the overall shape is consistent with the electron-microscopic map of MelB_{Ec}²⁴. The N- and C-terminal domains are related by a pseudo two-fold symmetry axis perpendicular to the membrane plane and separated from each other by an internal cavity facing the periplasm. Within each domain, there is a two-fold inverted pseudosymmetry between helices I–III and IV–VI, as well as between VII–IX and X–XII, forming repeats A–D (Supplementary Fig. S4c). Similar to other MFS members^{16,18,25}, MelB may have evolved from triple-helix repeats with a similar genetic origin.

Most MelB_{St} helices are irregular with kink(s) and tilts (Fig. 2b and Supplementary Figs S3 and S4). Two to three broken helices are observed in both molecules: helices IV, X and XI in Mol-A and helices II, VII and X in Mol-B. Mol-A exhibits a periplasmic-facing conformation with a partially occluded internal cavity due to the interactions between helices I and VII in the N- and

Table 1 | Data collection and refinement statistics (molecular replacement).

	MelB _{St}
Data collection	ALS 5.0.2
Space group	<i>P</i> ₃ ²
Cell dimensions	
<i>a</i> = <i>b</i> , <i>c</i> (Å)	127.20, 206.30
γ (°)	120.00
Resolution (Å)	40.00–3.35 (3.47–3.35)*
<i>R</i> _{sym} or <i>R</i> _{merge}	0.092 (0.77)
<i>I</i> / σ <i>I</i>	6.0 (1.52)
Completeness (%)	99.4 (99.4)
Redundancy	2.8 (2.7)
Refinement	
Resolution (Å)	38.0–3.35 (3.44–3.35)
No. of reflections	50,526
<i>R</i> _{work} / <i>R</i> _{free}	0.30/0.35
No. of atoms	
Protein	12,963
<i>B</i> -factors	
Protein	86.0
Root mean squared deviations	
Bond lengths (Å)	0.012
Bond angles (°)	1.7

MelB_{St}, *Salmonella typhimurium* melibiose permease.
*Values in parentheses are for highest-resolution shell.

C-terminal domains, respectively. This structure is described as an outward partially occluded conformation (Figs 2a and 5c). The cavity is closed on the cytoplasmic side by interdomain contacts between inner helices IV/X, V/VIII and II/XI; solvent is accessible from the periplasmic side. Mol-B has a partial outward opening compared with fully opened FucP²⁰, and is described as a partial outward conformation (Figs 2a and 5c). The root mean squared deviation between Mol-A and Mol-B is 2.7 Å, and the major differences are found in the first two helices of each repeat (Supplementary Fig. S4c), indicating that the inner helices move relatively independently between the two conformations.

Viewed from the periplasmic side, the internal cavity in Mol-A has an asymmetric charge distribution (Fig. 3a). Except for Lys377 in the C-terminal domain, all other charged residues, including Asp residues (19, 55, 59 and 124), Lys18 and Arg residues (52 and 149), are in the N-terminal domain. The calculated omit maps do not reveal interpretable densities for either bound sugar or cation.

The cation-binding site. A cluster of Asp residues at positions 55 and 59 (helix II), and 124 (helix IV), forms a pyramidal-shaped pocket in Mol-A (Fig. 3a and Supplementary Fig. S5a). In close proximity, there are Tyr120, Thr121 (helix IV) and Thr373 (XI). Together these residues could form the trigonal bipyramid geometry required for a metal-binding site^{26,27}. Thr121 forms H-bonds with Asn58 and Asp59, stabilizing the interaction between helices II/IV, and Lys377 H-bonds with Tyr120 separating the negatively charged pocket from the central water-filled cavity (Fig. 3a). Asp124 is buried between Tyr120 and Trp128. Asp59 is buried in a hydrophobic environment (Supplementary Fig. S5c).

Remarkably, Cys replacement at position 55, 59, 124, 58, or 121 differentially alters cation selectivity. Thus, the D55C mutant in MelB_{St} retains only a low level of H⁺-coupled melibiose binding and active transport (Fig. 3c,d and Supplementary Fig. S6a), but Na⁺ or Li⁺ does not stimulate either binding or transport. The D59C and D124C mutants bind ligand with reduced affinity

(Fig. 3d), but do not catalyse active melibiose transport (Fig. 3c and Supplementary Fig. S6a). Reduced rates of melibiose efflux and exchange are observed with mutant D59C, but mutant D124C does not exhibit exchange activity. In contrast to wild type (WT), melibiose binding, efflux and exchange in the D59C mutant are not stimulated by Na⁺ or Li⁺ nor is efflux inhibited at acidic pH (Fig. 4); thus, the D59C mutant behaves similar to a sugar uniporter. None of these mutations has an adverse effect on protein expression (Supplementary Fig. S6b). Furthermore, both the N58C and T121C mutations selectively inhibit H⁺- and Na⁺-coupled activity, with little effect on Li⁺-coupled melibiose transport (Fig. 3c and Supplementary Fig. S6a). Combined with the observed geometry and functional data presented here and elsewhere^{7,28–30}, we propose that the cation-binding site selectively coordinates Na⁺, Li⁺ or H₃O⁺ through a dynamic change in size and shape²⁷ dictated by the orientation of Asp55, Asp59 and Asp124. This supports the conclusion that all coupling cations in MelB compete for a single binding site^{4,13,14}. It is apparent that each Asp residue at these positions has a specific role in cation binding and coupling. All three Asp residues are required for Na⁺ or Li⁺ binding, and Asp59 is essential for H⁺ binding. Asp59 is buried in a hydrophobic environment (Supplementary Fig. S5c); based on the PROPKA prediction³¹, it has a largely elevated pKa of 9.0. We propose that Mol-A is in a protonated state. As the cation-binding site binds H⁺, Na⁺ or Li⁺ mutually exclusively^{4,13,14}, a bound Na⁺ is not expected in this configuration.

In Mol-B, the pyramidal-shaped cation-binding site is deformed. Displacement of the helix XI kink between helices II and IV places Asp55 and Asp59 in a different environment (Fig. 3b and Supplementary Fig. S5d), distorting the pyramidal arrangement. The deformation of the cation-binding site is probably necessary to release the bound Na⁺. This conformational change, which is involved in rearrangement of the helices, is expected to contribute to the rate-limiting step of transport^{4,9,32}. In this state, Arg52 holds helix XI by H-bonding with backbone atom of Gly378, indicating a primary structural role. Furthermore, Asp55 also stabilizes packing between helices II and XI.

The known crystal structures of other Na⁺-coupled symporters^{26,33,34} have a relatively low-affinity Na⁺-binding motif, where four to six partial charges coordinate Na⁺. In contrast, MelB utilizes three Asp residues representing a unique, higher-affinity Na⁺-binding motif^{4,29}.

The sugar-binding site. The sugar specificity of MelB_{St} is highly selective for di- or trisaccharides containing a D-galactopyranosyl moiety or the monosaccharide D-galactose, as in MelB_{Ec}⁸ or LacY^{35–37}. In close proximity to the cation-binding site, a water-filled cavity is observed between residues Asp19 (helix I), Arg149 (helix V), Tyr120, Asp124 and Trp128 (helix IV), as well as Lys377 (helix XI; Fig. 3a). Asp19 and Arg149 form a salt bridge on one side of the cavity; Tyr120 and Lys377 are H-bonded on the other side. Cys replacement at each of these positions abolishes or markedly decreases binding, as measured by Trp → D²G fluorescence resonance energy transfer (FRET), and melibiose transport (Fig. 3c,d, and Supplementary Figs S6 and S7), although mutant K377C retains 30–40% of WT symport activity with each cation (Fig. 3c and Supplementary Fig. S6a). In MelB_{Ec}, single-Cys mutation of Asp19 selectively abolishes sugar binding with little effect on Na⁺ binding³⁰, mutant W128F has decreased affinity for 4-nitrophenyl- α -D-galactopyranoside³⁸, and mutants Y120F and D124E exhibit decreased sugar- and Na⁺-binding affinities³⁹. Therefore, these charged or polar side chains, particularly Asp19 and Arg149, play critical roles in sugar

selectivity and affinity, and the aromatic residues Trp128 and Tyr120 may contribute to affinity by CH/ π -interactions with the pyranosyl ring of the sugar^{40,41}. Clearly, a crystal structure with bound sugar is required to determine the sugar-binding coordinates precisely. In Mol-B, the salt bridge between Asp19 and Arg149 is broken, and Trp128 is also displaced from the cavity, suggesting deformation of the sugar-binding site (Fig. 3b). It is noteworthy that the cation-binding site is also collapsed in this conformation; hence, the Mol-B probably represents an inactive state of MelB_{St}.

It is interesting that both LacY and MelB have similar sugar specificity and location of the sugar-recognition sites³⁵; however, their cation-binding sites are related by a pseudo two-fold symmetry axis perpendicular to the membrane plane. The

location of the Na⁺-binding site in MelB is away from Arg149, which is involved in sugar binding, thereby allowing the presence of a strongly negatively charged metal-binding site without a negative influence on sugar binding.

Positive cooperative binding between the cosubstrates is well established in MelB^{4,38,39,42}. Helix IV, in the middle of the N-terminal domain, physically connects both cosubstrate sites. In addition to Tyr120 and Asp124, Lys18 (Fig. 3c and Supplementary Fig. S6) H-bonds with the backbone atom of Met123 (Fig. 3a,b), which links helices I–IV, underscoring the crucial role of helix IV in cooperative binding and transport. On the basis of the structures, we anticipate that Na⁺ binding leads to movement of helix IV, which recruits Asp124, optimizing the pyramidal shape of the cavity with Asp55 and Asp59, and

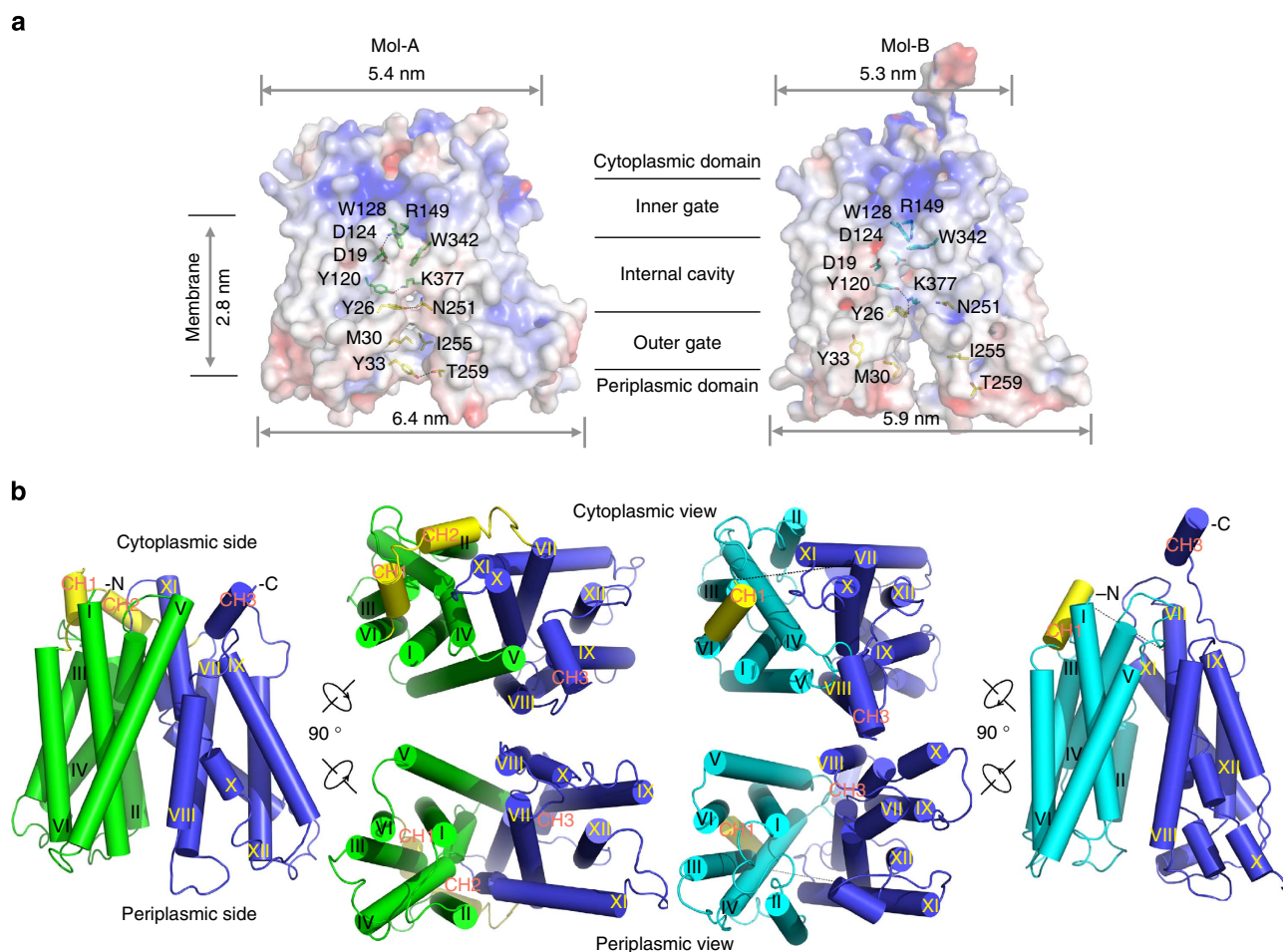
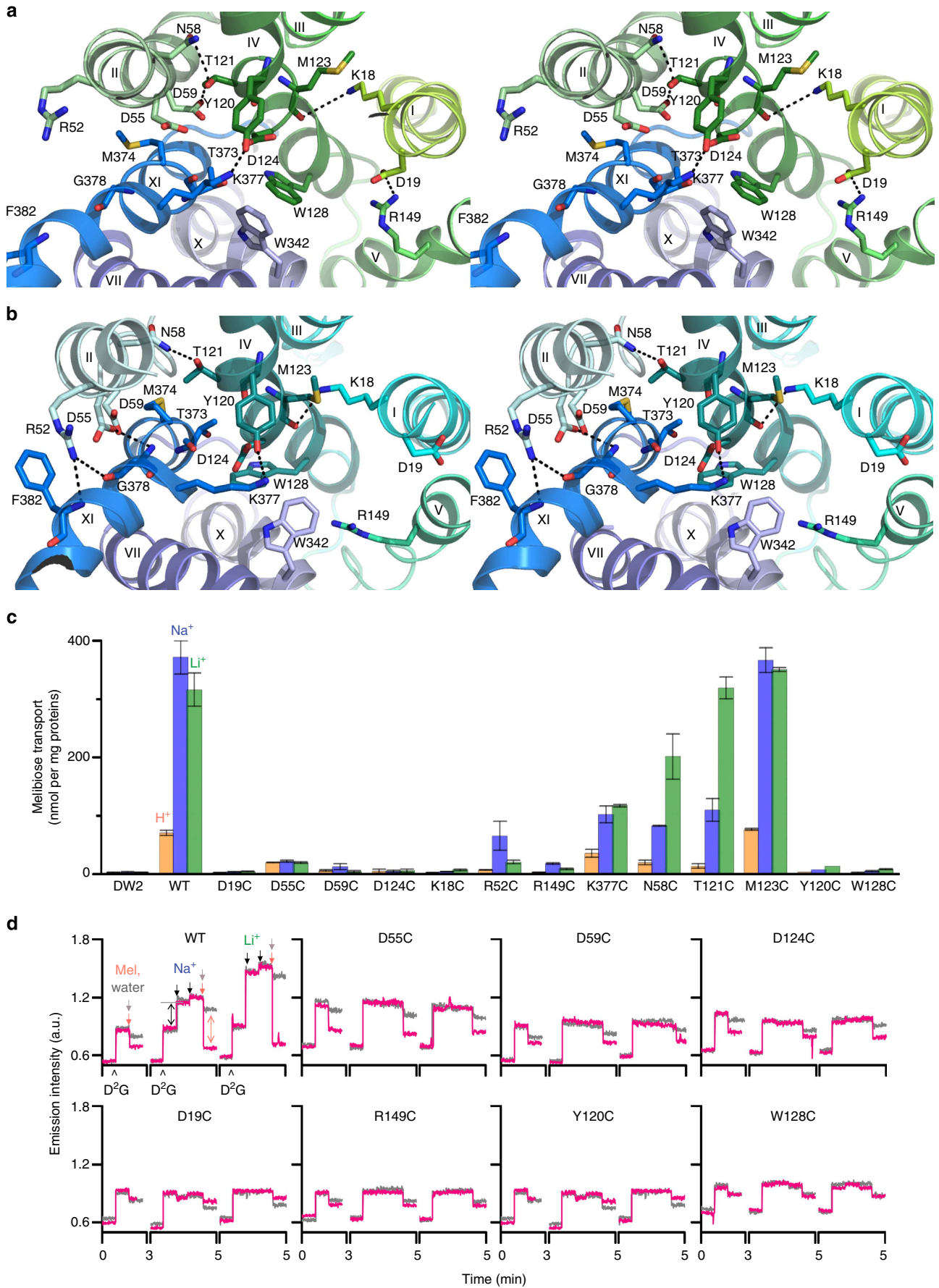


Figure 2 | Crystal structures of MelB_{St} in two outward conformations. (a) Surface electrostatic maps with side chains forming the outer gate and the internal cavity shown in yellow and green (Mol-A), respectively, or cyan (Mol-B) sticks. (b) Overall structure of MelB_{St}. The N-terminal domains of Mol-A or Mol-B are shown in green and cyan, respectively, and the central loops are shown in yellow. The helices are labelled with Roman numerals. CH1–3 denote the helices in the cytoplasmic loops and the C-terminal tail. All figures showing MelB structures were prepared by C α ^{1–430} superposition of Mol-B on Mol-A.

Figure 3 | Cosubstrate-binding sites. (a) Wall-eyed stereo view from the periplasmic side of the internal cavity in Mol-A with the N- and C-halves in green and blue, respectively. (b) Identical view of Mol-B with N- and C-halves in cyan and blue, respectively. (c) Steady-state levels of [³H]melibiose accumulation by intact cells at 10 min presented as histograms. DW2, cells without MelB. Error bar, s.e.m.; $n = 2$ for all mutants with a single-site mutation and $n = 10$ for the WT and DW2. (d) Trp \rightarrow D²G FRET with RSO vesicles. The emission signals were collected at wavelength of 490 nm after being excited at wavelength of 290 nm. \wedge , adding 10 μ M D²G; pink arrows \downarrow , adding 120 mM melibiose; grey arrows \downarrow , adding water; black arrows \downarrow , adding 20 mM or 50 mM Na⁺ or Li⁺. Black double-headed arrows \leftrightarrow , Na⁺ or Li⁺ stimulation; pink double-headed arrows \leftrightarrow , melibiose displacement of D²G.



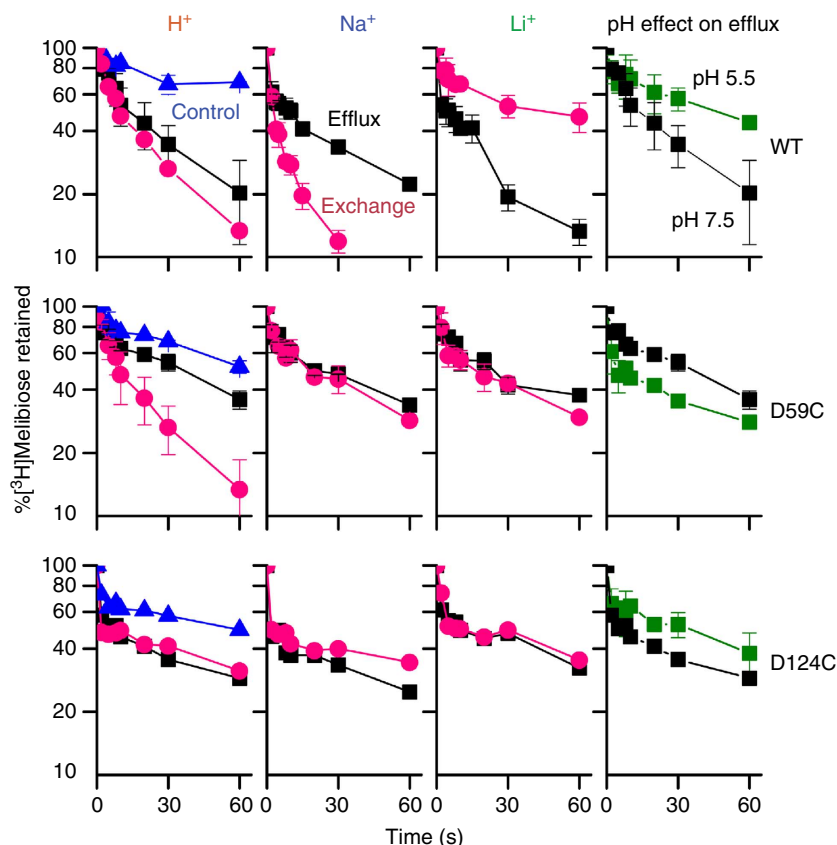


Figure 4 | Melibiose efflux and exchange. RSO membrane vesicles (28 mg ml^{-1}) containing MelB_{St} were tested for outwardly directed flow of [^3H]melibiose in the absence (efflux, squares) or presence (exchange, red circles) of equimolar concentration of unlabelled melibiose. The same experiment was performed in the presence of 20 mM NaCl or LiCl. 2-(4'-maleimidylanilino)naphthalene-6-sulphonic acid-treated vesicles were used for the negative control (blue triangles). Acidic pH effect on melibiose efflux was tested by decreasing the dilution buffer pH to 5.5 (green squares). Error bar, s.e.m., $n = 2$.

aligning Tyr120 and Trp128 for aromatic stacking with the sugar, thereby increasing affinity. It is well documented that sugar affinity is increased by more than threefold in the presence of Na⁺ or Li⁺ (refs 4,13,29,30,43), and Asp124 is required for completion for the Na⁺-binding site³⁰.

Ionic locks and conformational cycling. Both conformers are present in the same crystal, indicating that MelB_{St} has multiple conformations. Available crystal structures show MFS permeases in inward or outward conformations with occluded or partial-to-fully open cavities (Fig. 5), implying that an individual transporter may favour few conformers within a conformational cluster depending on the lowest free-energy state. The energy barrier for altering conformational equilibrium between inward and outward clusters may be the formation of an occluded intermediate state. Here we show that extramembrane electrostatic interactions play a crucial role in this regard.

Both inside-closed structures of MelB_{St} exhibit multiple hydrophobic interactions (hydrophobic patches) on the cytoplasmic side of the transmembrane helices sealing the cavity between N- and C-domains (Fig. 6a, left). This sealed dynamic domain is also stabilized by interdomain electrostatic interactions, designated as ionic locks, involving three Arg residues: Arg295 (cytoplasmic end of helix IX), Arg141 (cytoplasmic end of the helix V) and Arg363 (flexible loop₁₀₋₁₁; Fig. 6a,b). At the first ionic lock (L-1), Arg295 forms multiple H-bonds with Gln143 (helix V) and Pro287 (helix VIII) to hold helix V close to the

C-terminal domain. At L-2, Arg141 forms four H-bonded ion pairs with Asp351 and Asp354 (helix X), stabilizing helix X. At L-3, Arg363 (loop₁₀₋₁₁) forms one ion pair and two H-bonding interactions with the backbone atoms of Val204, Asp208 (N-terminal side of central loop₆₋₇) and Gly74 (loop₂₋₃), holding the N-terminal domain in an outward-facing conformation. It is likely to be that by stabilizing helix X, ionic locks L-1 and L-2 facilitate interaction of Arg363 with its partners. Replacing Arg363, Arg141 or Arg295 individually with Cys yields conformationally compromised mutants that fail to transport but retain affinity for both cosubstrates (Fig. 6c,d and Table 2). As indicated from a thread model of MelB_{St} at an inward-facing conformation (Fig. 6a, right), all three cytoplasmic interdomain locks are at an unlocked state, as the residues involved in these electrostatic interactions are 20 Å far apart. Therefore, these three ionic locks play important role in facilitating the formation of outward-facing conformation. On the periplasmic side, Asp35 (helix I) organizes L-4 (Fig. 6a,b) by forming a salt bridge and an H-bond with Arg175 (helix VI) and stabilizes the outward-facing conformation.

Discussion

Similar ionic lock interactions are present in other MFS structures (Fig. 5 and Supplementary Fig. S8). From top to bottom in the Fig. 5, conformations are depicted from the full-inward to the full-outward states^{17,18,20-23,44-46}. None of the predicted locks L-1, L-2 and L-3 exists in cluster-1, which includes the full and

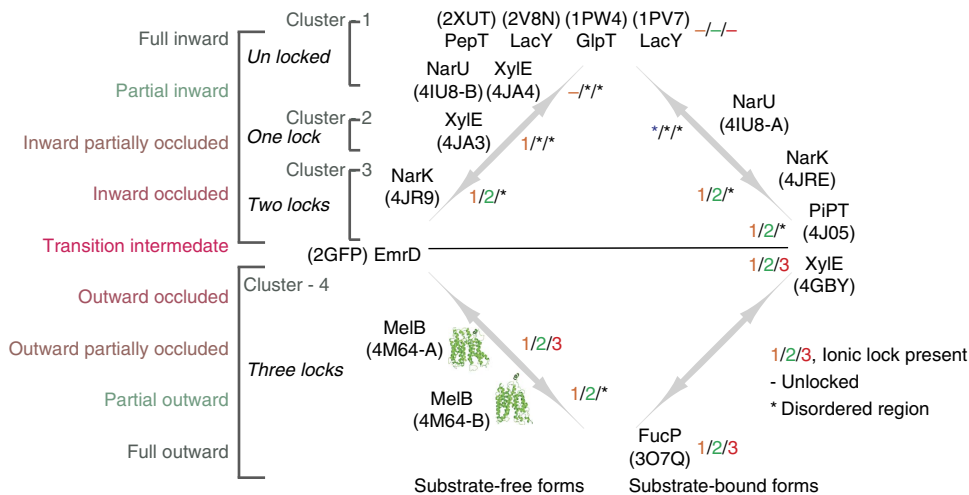


Figure 5 | Clusters of MFS permeases in different conformations. Structures were categorized into clusters according to their conformational state. *, Disordered region in structure; -, at an unlocked state; 1/2/3, the presence of lock-1, lock-2 or lock-3. PDB ID is shown for each structure.

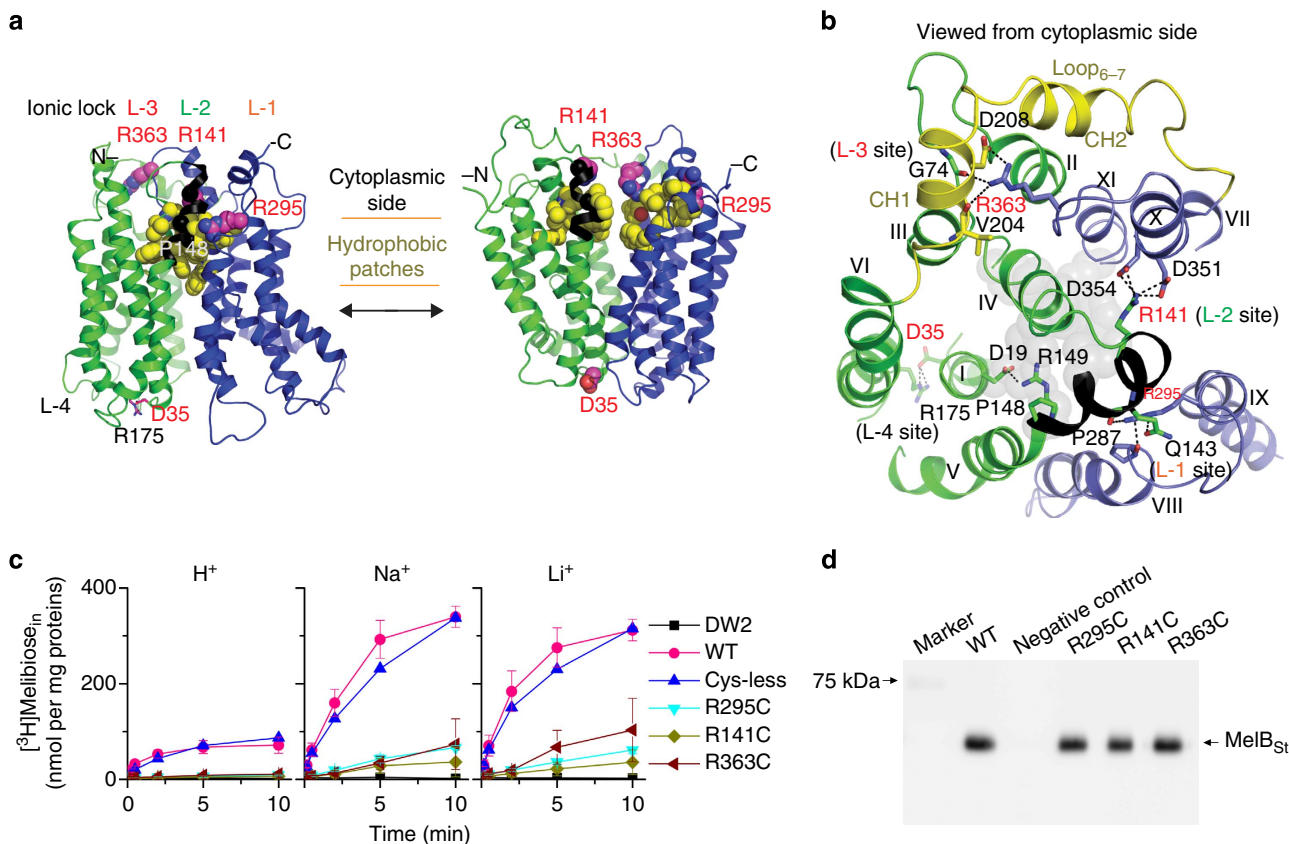


Figure 6 | Ionic locks and conformational cycling. N- and C-terminal domains are shown in green and blue, respectively, and hydrophobic patches are in yellow. Arg141-Arg149 stretch is coloured as black. 'L' denotes positions of ionic locks. (a) Left, outward partially occluded conformation (MolA); right, threading model for inward conformation. (b) Residues forming ionic locks are shown in sticks connected by broken lines. Grey spheres represent the residues involved in sugar binding. (c) Cys mutant of Arg residue at position 295, 141 or 363. Intact *E. coli* DW2 cells containing WT MelB_{St} or a given mutant were assayed for [³H]melibiose transport (0.4 mM, 10 mCi mmol⁻¹) in the absence or presence of 20 mM NaCl or LiCl. Intracellular melibiose expressed as nmol mg⁻¹ of total proteins is plotted as a function of time. Each single-site mutation is in the WT background. Error bar, s.e.m., n = 2 for the mutants and n = 3 for the WT. (d) Western blotting. Twenty-five micrograms of RSO vesicles was loaded on each well and detected by anti-His-tag antibody.

partially inward states. L-1 is formed in cluster-2, the inward partially occluded state. When the conformation reaches a more occluded state (cluster-3), both L-1 and L-2 are observed. L-3 is

not observed in any of the inward conformers, but exists in most outward structures (cluster-4). Thus, formation of an occluded state probably requires L-1 and L-2, and the outward state

Table 2 | Affinity for melibiose and Na⁺.

	Melibiose displacement of D ² G (IC ₅₀ , mM)	Na ⁺ activation constant for D ² G FRET (K _{0.5r} , mM)
WT MelB _{St}	2.65 ± 0.80*	1.92 ± 0.78
R295C	4.04 ± 0.42	3.22 ± 1.07
R141C	5.93 ± 1.61	4.77 ± 0.39
R363C	2.83 ± 0.57	5.51 ± 1.07

D²G, 2'-(N-dansyl)aminoalkyl-1-thio-β-D-galactopyranoside; FRET, fluorescence resonance energy transfer; MelB_{St}, *Salmonella typhimurium* melibiose permease; WT, wild type.
*s.e.m., n = 2.

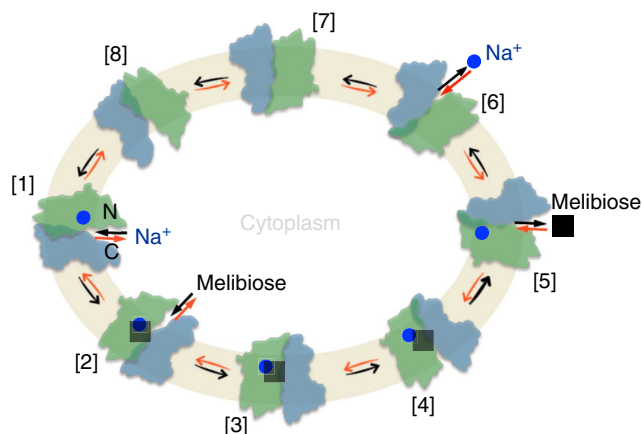


Figure 7 | Scheme for Na⁺/melibiose symport. [1–8], Kinetic steps in the overall transport cycle. The green colour-filled cycle represents the cell inner membrane. Na⁺, blue circles; melibiose, black squares. N, the N-terminal domain in green colour; C, the C-terminal domain in blue colour. Melibiose influx down a sugar concentration gradient starts at step [6] and proceeds via the red arrows around the circle, and melibiose efflux down a sugar concentration gradient starts at [1] and proceeds via the black arrows around the circle. Active transport of melibiose against a concentration gradient proceeds from step [6] via the red arrows as the melibiose influx.

requires all three ionic locks. Reverse order of lock formation is expected for the conformational changes to proceed in the opposite direction. The formation and deformation of these ionic interactions are the structural foundation for the function-required conformational switching between inward and outward conformers.

What triggers the locking/unlocking processes? In MelB, the salt bridge between Arg149 and Asp19 is involved in sugar binding. It is noteworthy that a short cytoplasmic stretch of helix V (Arg141–Arg149) links the sugar-binding site with two ionic locks (L-1 and L-2; Fig. 6a,b) and also contains two other conformationally important residues, Glu142 (ref. 42) and Pro148 (ref. 47). We propose that sugar binding promotes a dynamic state of the cytoplasmic stretch of helix V (Fig. 6a,b) and triggers locking/unlocking processes associated with a cascade of structural rearrangements for reorientation of the sugar-binding pocket.

We previously proposed a sequential binding kinetic model to explain reversible cation/melibiose symport in MelB based on an alternating-access mechanism (Fig. 7)^{9,12,42}. The structural and functional studies discussed here allow integration of the conformational states with kinetic steps in the proposed model for explaining melibiose/Na⁺ symport reactions. Although melibiose/Na⁺ efflux is explained for experimental simplicity⁴, influx is the reverse reaction starting from the intermediate [6]

(Fig. 7) and proceeds via the red arrows around the circle; active melibiose transport driven by $\Delta\tilde{\mu}_{\text{H}^+, \text{Na}^+ \text{ or } \text{Li}^+}$ is likely to occur in similar fashion. The polarity of transport is controlled by the direction of the net free energy stored in the form of either the sugar gradient or the electrochemical gradient of Na⁺, Li⁺ or H⁺, and the transport process is reversible.

This simplified scheme for melibiose efflux involves eight states (Fig. 7, black arrows): [1] inward Na⁺-bound state. Binding of a Na⁺ to the cation-binding site induces helix IV movement with an increase in sugar affinity. [2] Inward Na⁺- and melibiose-bound state. Sugar binding from the cytoplasm initiates the locking process (Fig. 6a,b). [3] Occluded Na⁺- and melibiose-bound state. Closure of the cytoplasmic cavity by the hydrophobic patch is locked by L-1 and L-2. [4] Outward Na⁺- and melibiose-bound state. Interactions at L-3 and L-4 facilitate a conformational transition from the occluded to an outward state. [5] Outward melibiose-released state. Bound melibiose is released to the periplasmic side from the open outer gate. The crystal structures of MelB_{St} suggest that the cation exits via the internal cavity that contains the sugar-binding site and that a bound sugar should restrain the dynamics of the bound cation; therefore, release of sugar is a prerequisite for releasing Na⁺. The structural basis for the ordered release is supported by kinetic studies^{4,11} and the behaviour of mutant G117R⁹, which catalyses melibiose exchange but no reaction involving net Na⁺ transport, that is, involving only steps [1] \rightleftharpoons [5]. [6] Outward Na⁺-released state. Deformation of the cation-binding site facilitates Na⁺ release as suggested by the Mol-B structure (Fig. 3b). [7] Occluded-empty state. Formation of the unloaded intermediate state occluded on both sides. [8] Inward-empty state. Once the cavity is open to the cytoplasm, the next transport cycle begins. Melibiose efflux involves the whole cycle with one sugar and one charge moving across the membrane. In contrast, melibiose exchange involves only states [1–5].

Interestingly, it appears that the kinetic model is similar for different MFS permeases regardless of the coupling cation^{35,48,49}. In the solely H⁺-coupled LacY^{50–53}, it is well established that at physiological pH, LacY is protonated⁵². Sugar binds only to protonated LacY^{50,53} and dissociates before the release of H⁺ during symport⁵⁰. The inward-facing crystal structures of LacY^{16,17} indicate that the sugar-binding site is coupled to the H⁺-binding site through an electrostatic network; as a result, the affinity for the sugar binding is optimized in a protonated state. A similar coupling phenomenon is observed in MelB. The comparison of the structures of Mol-A and Mol-B reveals that a protonated cation-binding site is coupled with a properly formed sugar-binding pocket, and the deformation of the cation-binding site induces deformation of the sugar-binding site. In LacY, the H⁺ may involve in a single side chain (for example, Glu325)^{16,17,35,54}; in MelB, the H⁺ may be bound in different forms, a protonated side chain (for example, Asp59) or as H₃O⁺ that is shared by Asp55, Asp59 and Asp124 in the metal-binding cavity. Possibly, these two protonation forms represent different states of bound H⁺ in MelB.

What is the effect of Na^+ or Li^+ on MelB? In general, binding of Na^+ or Li^+ requires four to six coordination numbers from two to three helices, and the small ionic radius of Na^+ and Li^+ require the coordination ligands in closer distance. Thus, metal binding should induce a relatively large change in movement of helices. On the basis of the structures of MelB_{St}, it is anticipated that Na^+ binding recruits Asp124 to complete Na^+ binding, resulting in movement of helix IV with Tyr120 and Trp128 for aromatic stacking with the bound sugar. It is well known that sugar affinity is largely increased by aromatic stacking in LacY⁴⁰. According to this notion, Na^+ and Li^+ are more effective ‘activators’ than H^+ . This structural interpretation is consistent with the previous conclusion derived from functional studies of MelB_{Ec}^{30,32,38}. Therefore, it is likely to be that an essential aspect of coupling is that binding of the cation activates the substrate-binding site, a property that is conserved in both MelB and LacY.

What prevents cation leakage in MelB? The opening and closing of the cytoplasmic side to form the substrate exit pathway involves dynamics of cytoplasmic helix V in MelB (Fig. 6a,b), which is initiated only by sugar binding. In the absence of sugar, ‘the leader’, MelB/ Na^+ complexes should preferentially populate outward conformations. This structural arrangement can prevent bound Na^+ from futile cycling and also offers an explanation for how the extramembrane ionic locks, as ‘the follower’, respond to the primary effect of sugar binding in the middle of the molecule.

Methods

Large-scale protein production. Full-length MelB_{St} encoded by plasmid pK95 $\Delta\text{AH}/\text{MelB}_{\text{St}}/\text{CHis}_{10}$ (refs 4,55) with Leu5→Met and a His₁₀ tag at the C terminus (namely the WT) was expressed in *E. coli* DW2 strain (*mela*⁺, ΔmelB and ΔlacZY)⁵⁵. In a 10-l fermenter, cells were grown in Luria–Bertani (LB) broth supplemented with 50 mM KP_i (pH 7.0), 45 mM (NH₄)₂PO₄, 0.5% glycerol and 100 mg l⁻¹ ampicillin at 30 °C until they approached stationary phase at A₆₀₀ of ~3.3. Cells with constitutively overexpressed MelB_{St} were then harvested, resuspended in 20 mM Tris–HCl (pH 7.5), 200 mM NaCl and 10% glycerol, broken with an EmulsiFlex instrument and centrifuged at 20,000 g for 15 min to remove unbroken cells⁵⁶. Membranes were harvested from the supernatant by ultracentrifugation at 144,651 g for 3 h in a Beckman rotor, type 45 Ti. The pellets were resuspended in the same buffer, frozen in liquid N₂ and stored at -80 °C. The protein concentration of the membrane samples was assayed using Micro BCA Protein Assay Kit (Pierce).

Protein purification. Membranes (14 mg ml⁻¹) were extracted with 1.5% n-undecyl-β-D-maltoside (UDM) followed by ultracentrifugation at 265,000 g for 30 min. Purification was performed by cobalt-affinity chromatography (TALON resins). The column was pre-equilibrated with 50 mM NaP_i (pH 7.6), 200 mM NaCl, 10% glycerol, 0.035% UDM, 5 mM imidazole. After loading and washing the column with 35 mM imidazole buffer, MelB_{St} was eluted with buffer containing 200 mM imidazole, concentrated with VIVASPIN 20 (50 kDa cutoff value), dialysed twice against 1 litre of 20 mM Tris–HCl (pH 7.5), 100 mM NaCl, 10% glycerol, 0.035% UDM, further concentrated to >20 mg ml⁻¹, and finally ultracentrifuged at >360,000 g for 45 min. The protein was flash-frozen in liquid nitrogen and stored at -80 °C. From a 10-l culture, highly purified MelB_{St} at 30–40 mg was obtained routinely.

Isothermal titration calorimetry. ITC measurements were performed in a nano isothermal titration calorimeter (TA Instruments). The purified MelB_{St} in the dialysis buffer was injected into the ITC sample cell and 6 mM melibiose dissolved in the same dialysis buffer was titrated incrementally into the protein sample, and the heat rate was recorded at 25 °C. Melibiose binding was also measured in the presence of 100 mM LiCl. The cumulative heat change (ΔQ) was plotted against the molar ratio of melibiose to MelB_{St} and fitted with the one-site independent binding model (NanoAnalyse software).

Protein expression for functional studies. *E. coli* DW2 cells containing a given plasmid were grown in LB broth with 100 mg l⁻¹ of ampicillin at 37 °C. The overnight cultures were diluted by 5% to LB broth supplemented with 0.5% glycerol and 100 mg l⁻¹ of ampicillin, and the constitutive overexpression was obtained by shaking at 30 °C for another 5 h.

Preparation of right-side-out membrane vesicles. RSO membrane vesicles were prepared from *E. coli* DW2 cells by osmotic lysis^{4,57,58}. Cells were incubated with

50 μg ml⁻¹ lysozyme in the presence of 10 mM EDTA (pH 7.5), 5 mM dithiothreitol (DTT) and 30% (w/v) sucrose for 45 min; the yielded spheroplasts were harvested by centrifugation at 14,000 g for 40 min at 4 °C and suspended with 20-ml cocktail containing 100 mM KP_i (pH 7.5), 20 mM MgSO₄, 30% sucrose, 5 mM DTT, 1 mg ml⁻¹ deoxyribonuclease and 1 mg ml⁻¹ ribonuclease. The resuspended spheroplasts were lysed by rapid dilution into 1-litre 50 mM KP_i (pH 7.5) buffer with 5 mM DTT, and the solution was incubated at 37 °C for 10 min. After further incubation with 10 mM EDTA (pH 7.0) for 10 min and 15 mM MgSO₄ for another 10 min, the total membrane vesicles were harvested by centrifugation at 14,000 g for 25 min at 4 °C. The RSO vesicles were collected from the supernatant after centrifugation at 800g for 12 min at 4 °C, then extensively washed and resuspended with 100 mM KP_i (pH 7.5) at a protein concentration of ~20–28 mg ml⁻¹, frozen in liquid N₂ and stored at -80 °C.

Melibiose transport assay with intact cells. Melibiose active transport with intact cells were carried out with [³H]melibiose⁴, which was custom synthesized by PerkinElmer (Boston, MA). *E. coli* DW2 cells expressing MelB_{St} were washed with 50 ml of 100 mM KP_i (pH 7.5), so-called Na^+ -free buffer. The cell pellets were resuspended with 100 mM KP_i (pH 7.5) and 10 mM MgSO₄, adjusted to an A₄₂₀ = 10 (~0.7 mg protein ml⁻¹) and aliquoted with 50 μl. Transport was initiated by adding 2 μl of [³H]melibiose with a specific activity of 10 mCi mmol⁻¹ at a final concentration of 0.4 mM in the absence or presence of either 20 mM NaCl or LiCl, and stopped at a given incubation time. Intracellular melibiose was assayed by a fast filtration.

Melibiose efflux and exchange assays. RSO membrane vesicles containing the WT or a mutant MelB_{St} in 100 mM KP_i (pH 7.5) and 10 mM MgSO₄ were concentrated to ~28 mg ml⁻¹ and pre-equilibrated overnight on ice with 20 mM [³H]melibiose (10 mCi mmol⁻¹), 0.75 μM monensin and 10 μM carbonylcyanide m-chlorophenylhydrazone^{4,9,11}, without or with 20 mM NaCl or LiCl. Aliquots (2 μl) were diluted 200-fold into a given buffer in the absence (efflux) or presence (exchange) of 20 mM unlabelled melibiose⁵⁰, and reactions were terminated by dilution and rapid filtration at a given time.

Western blotting. Twenty-five micrograms of RSO membranes were loaded onto each well of SDS-16% PAGE. After transfer onto the polyvinylidene difluoride membrane, MelB_{St} proteins were detected with anti-His-tag antibody and imaged by the ImageQuant LAS 4000 Biomolecular Imager (GE Health Care Life Science)⁴⁷.

Trp→D²G FRET. D²G (refs 4,9,43,47,59) was used to test affinity for the cosubstrate via FRET from Trp residues to the dansyl moiety of the D²G bound with MelB_{St}. Steady-state fluorescence measurements were performed in a 3-mm quartz cuvette (Hitachi F-7000 Fluorescence Spectrophotometer or AMINCO-Bowman Series 2 Spectrometer).

The purified sugar-free MelB_{St} (1 μM) in the dialysis buffer or the buffer with 100 mM LiCl instead of NaCl was excited at wavelength of 290 nm and the emission fluorescence was recorded between 415 and 575 nm. With 10 μM D²G (the K_D value for the WT⁴), displacement of D²G bound by MelB_{St} was carried out by adding 50 mM melibiose, methyl-β-D-thiogalactoside, glucose or sucrose, respectively. The difference spectra before and after the addition of a given sugar for displacement (ΔI) is calculated and plotted.

The RSO membrane vesicles prepared from DW2 cells expressing MelB_{St} (1 mg ml⁻¹)^{4,9} in 100 mM KP_i (pH 7.5) were excited at wavelength of 290 nm; the emission fluorescence at wavelength of 490 nm was recorded for 1 min after each of the following addition unless specified: (1) 10 μM D²G; (2) 20 mM NaCl or LiCl; (3) 50 mM NaCl or LiCl; (4) 120 mM melibiose or same volume of water.

Half-maximal displacement of bound D²G (IC₅₀). Melibiose was added stepwise to the samples containing the RSO vesicles with D²G (10 μM) and 20 mM NaCl until no change in fluorescence emission occurred. The decrease in fluorescent intensity after each addition was corrected by the water dilution and was plotted as a function of melibiose concentration. The IC₅₀ value was determined by fitting a hyperbolic function to the data (OriginPro).

Na⁺-stimulation constant (K_{0.5}) for D²G FRET. Applying the same experimental setup, NaCl was consecutively added to the sample containing the RSO vesicles and D²G (10 μM)⁹. An identical volume of water was used for the control. Fluorescent increase (ΔI , the difference before (I₀) and after the addition of NaCl) was expressed as the percentage of the I₀, corrected by a dilution effect, and then plotted as a function of Na⁺ concentration. The K_{0.5} for Na⁺ stimulation was determined by fitting a hyperbolic function to the data (OriginPro).

Mutagenesis. All MelB_{St} mutants were constructed with the QuickChange Site-Directed Mutagenesis Kits (Stratagene) using the plasmid pK95 $\Delta\text{AH}/\text{MelB}_{\text{St}}/\text{CHis}_{10}$ as the template⁴.

Gel filtration chromatography. Gel filtration was performed in a Superdex 200 10/300 GL column on a Fast Protein Liquid Chromatography instrument. For the stability studies, the protein sample was placed at 23 °C for 5 days and analysed by the gel filtration chromatography and the D²G FRET assay.

Precrystallization phospholipid treatment. Before setting up crystallization trials, the protein samples were thawed out from –80 °C, ultracentrifuged at 384,492 g for 45 min at 4 °C (Beckman Coulter Optima MAX, TLA-100 rotor), diluted to a final protein concentration of 7 mg ml⁻¹ and incubated with phospholipids at a concentration of 3.3 mM (*E. coli* Extract Polar, Avanti, 100600) from a 15-mM stock dissolved with the dialysis buffer.

Crystallization, data collection and processing. Crystallization of MelB_{St} was carried out by the hanging-drop vapour-diffusion method at 23 °C by mixing 2 µl of phospholipid-treated protein samples⁶⁰ containing 5 mM αNPG (4-nitrophenyl-α-D-galactopyranoside) with 2 µl reservoir containing 100 mM 2-(N-morpholino) ethanesulfonic acid (pH 6.5), 100 mM NaCl, 50 mM CaCl₂, 35–37% PEG 400 and 0.08% octyl-β-D-galactopyranoside. Crystals were frozen with liquid nitrogen and tested for X-ray diffraction at the Lawrence Berkeley National Laboratory, ALS BL 8.2.1, 8.2.2, 5.0.1, 5.0.2 or at the Stanford Synchrotron Radiation Light Source BL 7-1 via remote data collection. The complete diffraction data set was collected at 100 K from a single cryocooled crystal at wavelength of 1.004 Å with an ADSC QUANTUM 315 detector at ALS BL 5.0.2; image data were processed with HKL 2000 (ref. 61) to a resolution of 3.35 Å with 98% completeness (Table 1).

Structure solution and refinement. Data were processed in space groups *P*₃₂₁, *P*₃₁₂, *P*₃₂ and *P*₃₁. The data set was analysed by Structure Factor Check on CCP4 (ref. 62) suite and Phenix Xtriage^{63,64}, which indicated a strong off-origin peak at 0, 0, 0.5 along *c** axis and also revealed merohedral twinning with twin fraction of 0.41 for the data processed in space groups *P*₃₂ and *P*₃₁. Search probes were prepared using the server I-TASSER⁶⁵, using the structures of MFS permeases, the inward LacY (PDB, 2V8N) and GlpT (1PW4), the occluded EmrD (2GFP), as well as the outward FucP (3O7Q). Using Phaser 2.52 programme⁶⁶ in Phenix suite, a single copy of each threading model with deletion of the longer loop_{6–7} and loop_{10–11}, and the C-terminal tail was used as the search probe to test the data processed in all space groups. Applying the native Patterson map and omit map to assist the molecular replacement processes, a maximal solution from the FucP-based MelB_{St} model was identified, and the crystal symmetry was determined to be *P*₃₂ containing two additional pseudocrystallographic symmetries with 74% solvent content.

The asymmetric unit contains four closely aligned molecules with two types of pseudo two-fold symmetry (twinning) along the *b* axis, with Mol-A and Mol-B related by 172°, and Mol-C and Mol-D related by 160° (Supplementary Fig. S3). Mol-AB and Mol-CD are related by 0.5 pseudotranslation. Twin refinement was carried out by REFMAC 5.7 programme using the Jelly-Body-Restrained refinement option in CCP4 suite with the twinning operator *k*, *h*, *-l*. Initial refinement yielded *R*/*R*_{free} of 0.37/0.42. Model verification was done by systematic calculation of omit maps at various regions. With iterative rounds of manual model building followed by simulated annealing and density modification, an interpretable density map to 3.35 Å resolution was obtained allowing assignment of most side chains for Mol-A and Mol-B (Supplementary Figs S3c,d and S5a,b). Final refinement was carried out using the Tangent Least-Square Jelly-Body-Restrained twin refinement, where the *R*/*R*_{free} values dropped to 0.30/0.35 (Table 1). As pseudosymmetries are present, higher apparent *R*/*R*_{free} values are expected⁶⁷. Out of 476 residues, 1–432 in Mol-A, regions 1–210 and 235–450 in Mol-B, 1–431 in Mol-C, as well as 1–100, 109–210, 235–398 and 408–431 in Mol-D, were well resolved. Residues (82.2%) are in most favoured, 17.4% in generously allowed and 0.4% in disallowed regions. Visualization of omit maps and manual model building were performed using Coot 0.7 (ref. 68). Surface electrostatic maps were calculated using APBS software⁶⁹. All crystallographic figures were generated with Pymol 1.5 (ref. 70).

References

- Poolman, B. *et al.* Cation and sugar selectivity determinants in a novel family of transport proteins. *Mol. Microbiol.* **19**, 911–922 (1996).
- Saier, Jr. M. H. Families of transmembrane sugar transport proteins. *Mol. Microbiol.* **35**, 699–710 (2000).
- Mizushima, K. *et al.* Cloning and sequencing of the *melB* gene encoding the melibiose permease of *Salmonella typhimurium* LT2. *Mol. Gen. Genet.* **234**, 74–80 (1992).
- Guan, L., Nurva, S. & Ankeshwarapu, S. P. Mechanism of melibiose/cation symport of the melibiose permease of *Salmonella typhimurium*. *J. Biol. Chem.* **286**, 6367–6374 (2011).
- Reiling, J. H. *et al.* A haploid genetic screen identifies the major facilitator domain containing 2A (MFSD2A) transporter as a key mediator in the response to tunicamycin. *Proc. Natl Acad. Sci. USA* **108**, 11756–11765 (2011).
- Saier, Jr. M. H. *et al.* The major facilitator superfamily. *J. Mol. Microbiol. Biotechnol.* **1**, 257–279 (1999).
- Wilson, T. H. & Ding, P. Z. Sodium-substrate cotransport in bacteria. *Biochim. Biophys. Acta* **1505**, 121–130 (2001).
- Wilson, D. M. & Wilson, T. H. Cation specificity for sugar substrates of the melibiose carrier in *Escherichia coli*. *Biochim. Biophys. Acta* **904**, 191–200 (1987).
- Guan, L., Jakkula, S. V., Hodkoff, A. A. & Su, Y. Role of Gly117 in the cation/melibiose symport of MelB of *Salmonella typhimurium*. *Biochemistry* **51**, 2950–2957 (2012).
- Niia, S., Moriyama, Y., Futai, M. & Tsuchiya, T. Cation coupling to melibiose transport in *Salmonella typhimurium*. *J. Bacteriol.* **144**, 192–199 (1980).
- Basiliana, M., Pourcher, T. & Leblanc, G. Facilitated diffusion properties of melibiose permease in *Escherichia coli* membrane vesicles. Release of co-substrates is rate limiting for permease cycling. *J. Biol. Chem.* **262**, 16865–16870 (1987).
- Basiliana, M., Pourcher, T. & Leblanc, G. Melibiose permease of *Escherichia coli*. Characteristics of co-substrates release during facilitated diffusion reactions. *J. Biol. Chem.* **263**, 9663–9667 (1988).
- Damiano-Forano, E., Basiliana, M. & Leblanc, G. Sugar binding properties of the melibiose permease in *Escherichia coli* membrane vesicles. Effects of Na⁺ and H⁺ concentrations. *J. Biol. Chem.* **261**, 6893–6899 (1986).
- Mus-Veteau, I., Pourcher, T. & Leblanc, G. Melibiose permease of *Escherichia coli*: substrate-induced conformational changes monitored by tryptophan fluorescence spectroscopy. *Biochemistry* **34**, 6775–6783 (1995).
- Yousef, M. S. & Guan, L. A 3D structure model of the melibiose permease of *Escherichia coli* represents a distinctive fold for Na⁺ symporters. *Proc. Natl Acad. Sci. USA* **106**, 15291–15296 (2009).
- Abramson, J. *et al.* Structure and mechanism of the lactose permease of *Escherichia coli*. *Science* **301**, 610–615 (2003).
- Guan, L., Mirza, O., Verner, G., Iwata, S. & Kaback, H. R. Structural determination of wild-type lactose permease. *Proc. Natl Acad. Sci. USA* **104**, 15294–15298 (2007).
- Huang, Y., Lemieux, M. J., Song, J., Auer, M. & Wang, D. N. Structure and mechanism of the glycerol-3-phosphate transporter from *Escherichia coli*. *Science* **301**, 616–620 (2003).
- Yin, Y., He, X., Szewczyk, P., Nguyen, T. & Chang, G. Structure of the multidrug transporter EmrD from *Escherichia coli*. *Science* **312**, 741–744 (2006).
- Dang, S. *et al.* Structure of a fucose transporter in an outward-open conformation. *Nature* **467**, 734–738 (2010).
- Sun, L. *et al.* Crystal structure of a bacterial homologue of glucose transporters GLUT1-4. *Nature* **490**, 361–366 (2012).
- Pedersen, B. P. *et al.* Crystal structure of a eukaryotic phosphate transporter. *Nature* **496**, 533–536 (2013).
- Newstead, S. *et al.* Crystal structure of a prokaryotic homologue of the mammalian oligopeptide-proton symporters, PepT1 and PepT2. *EMBO J.* **30**, 417–426 (2011).
- Purhonen, P., Lundback, A. K., Lemmonier, R., Leblanc, G. & Hebert, H. Three-dimensional structure of the sugar symporter melibiose permease from cryo-electron microscopy. *J. Struct. Biol.* **152**, 76–83 (2005).
- Madej, M. G., Dang, S., Yan, N. & Kaback, H. R. Evolutionary mix-and-match with MFS transporters. *Proc. Natl Acad. Sci. USA* **110**, 5870–5874 (2013).
- Yamashita, A., Singh, S. K., Kawate, T., Jin, Y. & Gouaux, E. Crystal structure of a bacterial homologue of Na⁺/Cl⁻-dependent neurotransmitter transporters. *Nature* **437**, 215–223 (2005).
- Kovalevsky, A. Y. *et al.* Identification of the elusive hydronium ion exchanging roles with a proton in an enzyme at lower pH values. *Angew. Chem. Int. Ed. Engl.* **50**, 7520–7523 (2011).
- Zani, M. L., Pourcher, T. & Leblanc, G. Mutagenesis of acidic residues in putative membrane-spanning segments of the melibiose permease of *Escherichia coli*. II. Effect on cationic selectivity and coupling properties. *J. Biol. Chem.* **268**, 3216–3221 (1993).
- Pourcher, T., Zani, M. L. & Leblanc, G. Mutagenesis of acidic residues in putative membrane-spanning segments of the melibiose permease of *Escherichia coli*. I. Effect on Na⁺-dependent transport and binding properties. *J. Biol. Chem.* **268**, 3209–3215 (1993).
- Granell, M., Leon, X., Leblanc, G., Padros, E. & Lorenz-Fonfria, V. A. Structural insights into the activation mechanism of melibiose permease by sodium binding. *Proc. Natl Acad. Sci. USA* **107**, 22078–22083 (2010).
- Bas, D. C., Rogers, D. M. & Jensen, J. H. Very fast prediction and rationalization of pK_a values for protein-ligand complexes. *Proteins* **73**, 765–783 (2008).
- Pourcher, T., Basiliana, M., Sarkar, H. K., Kaback, H. R. & Leblanc, G. The melibiose/Na⁺ symporter of *Escherichia coli*: kinetic and molecular properties. *Phil. Trans. R. Soc. Lond. Ser. B Biol. Sci.* **326**, 411–423 (1990).
- Faham, S. *et al.* The crystal structure of a sodium galactose transporter reveals mechanistic insights into Na⁺/sugar symport. *Science* **321**, 810–814 (2008).
- Ressl, S., Terwisscha van Scheltinga, A. C., Vonrhein, C., Ott, V. & Ziegler, C. Molecular basis of transport and regulation in the Na⁺/betaine symporter BetP. *Nature* **458**, 47–52 (2009).

35. Guan, L. & Kaback, H. R. Lessons from lactose permease. *Annu. Rev. Biophys. Biomol. Struct.* **35**, 67–91 (2006).
36. Guan, L., Sahin-Toth, M. & Kaback, H. R. Changing the lactose permease of *Escherichia coli* into a galactose-specific symporter. *Proc. Natl Acad. Sci. USA* **99**, 6613–6618 (2002).
37. Guan, L., Sahin-Toth, M., Kalai, T., Hideg, K. & Kaback, H. R. Probing the mechanism of a membrane transport protein with affinity inactivators. *J. Biol. Chem.* **278**, 10641–10648 (2003).
38. Cordat, E., Leblanc, G. & Mus-Veteau, I. Evidence for a role of helix IV in connecting cation- and sugar-binding sites of *Escherichia coli* melibiose permease. *Biochemistry* **39**, 4493–4499 (2000).
39. Zani, M. L., Pourcher, T. & Leblanc, G. Mutation of polar and charged residues in the hydrophobic NH₂-terminal domains of the melibiose permease of *Escherichia coli*. *J. Biol. Chem.* **269**, 24883–24889 (1994).
40. Guan, L., Hu, Y. & Kaback, H. R. Aromatic stacking in the sugar binding site of the lactose permease. *Biochemistry* **42**, 1377–1382 (2003).
41. Vazquez-Ibar, J. L., Guan, L., Svrakic, M. & Kaback, H. R. Exploiting luminescence spectroscopy to elucidate the interaction between sugar and a tryptophan residue in the lactose permease of *Escherichia coli*. *Proc. Natl Acad. Sci. USA* **100**, 12706–12711 (2003).
42. Meyer-Lipp, K. *et al.* The inner interhelix loop 4-5 of the melibiose permease from *Escherichia coli* takes part in conformational changes after sugar binding. *J. Biol. Chem.* **281**, 25882–25892 (2006).
43. Maehrel, C., Cordat, E., Mus-Veteau, I. & Leblanc, G. Structural studies of the melibiose permease of *Escherichia coli* by fluorescence resonance energy transfer. I. Evidence for ion-induced conformational change. *J. Biol. Chem.* **273**, 33192–33197 (1998).
44. Qvistgaard, E. M., Low, C., Moberg, P., Tresaugues, L. & Nordlund, P. Structural basis for substrate transport in the GLUT-homology family of monosaccharide transporters. *Nat. Struct. Mol. Biol.* **20**, 766–768 (2013).
45. Yan, H. *et al.* Structure and mechanism of a nitrate transporter. *Cell Rep.* **3**, 716–723 (2013).
46. Zheng, H., Wisedchaisri, G. & Gonen, T. Crystal structure of a nitrate/nitrite exchanger. *Nature* **497**, 647–651 (2013).
47. Jakkula, S. V. & Guan, L. Reduced Na⁺ affinity increases turnover of *Salmonella enterica* serovar Typhimurium MelB. *J. Bacteriol.* **194**, 5538–5544 (2012).
48. Doki, S. *et al.* Structural basis for dynamic mechanism of proton-coupled symport by the peptide transporter POT. *Proc. Natl Acad. Sci. USA* **110**, 11343–11348 (2013).
49. Madej, M. G., Soro, S. N. & Kaback, H. R. Apo-intermediate in the transport cycle of lactose permease (LacY). *Proc. Natl Acad. Sci. USA* **109**, E2970–E2978 (2012).
50. Kaczorowski, G. J. & Kaback, H. R. Mechanism of lactose translocation in membrane vesicles from *Escherichia coli*. I. Effect of pH on efflux, exchange, and counterflow. *Biochemistry* **18**, 3691–3697 (1979).
51. Smirnova, I., Kasho, V., Sugihara, J., Choe, J. Y. & Kaback, H. R. Residues in the H⁺ translocation site define the pK_a for sugar binding to LacY. *Biochemistry* **48**, 8852–8860 (2009).
52. Smirnova, I. N., Kasho, V. & Kaback, H. R. Protonation and sugar binding to LacY. *Proc. Natl Acad. Sci. USA* **105**, 8896–8901 (2008).
53. Smirnova, I., Kasho, V., Sugihara, J., Vazquez-Ibar, J. L. & Kaback, H. R. Role of protons in sugar binding to LacY. *Proc. Natl Acad. Sci. USA* **109**, 16835–16840 (2012).
54. Carrasco, N. *et al.* Characterization of site-directed mutants in the lac permease of *Escherichia coli*. 2. Glutamate-325 replacements. *Biochemistry* **28**, 2533–2539 (1989).
55. Pourcher, T., Leclercq, S., Brandolin, G. & Leblanc, G. Melibiose permease of *Escherichia coli*: large scale purification and evidence that H⁺, Na⁺, and Li⁺ sugar symport is catalyzed by a single polypeptide. *Biochemistry* **34**, 4412–4420 (1995).
56. Chae, P. S. *et al.* Maltose-neopentyl glycol (MNG) amphiphiles for solubilization, stabilization and crystallization of membrane proteins. *Nat. Methods* **7**, 1003–1008 (2010).
57. Kaback, H. R. in *Methods in Enzymology* Vol. XXII (eds Kaplan, Nathan P., Jakoby, William B. & Colowick, Nathan P.) 99–120 (Elsevier, 1971).
58. Short, S. A., Kaback, H. R. & Kohn, L. D. D-lactate dehydrogenase binding in *Escherichia coli dld*- membrane vesicles reconstituted for active transport. *Proc. Natl Acad. Sci. USA* **71**, 1461–1465 (1974).
59. Cordat, E., Mus-Veteau, I. & Leblanc, G. Structural studies of the melibiose permease of *Escherichia coli* by fluorescence resonance energy transfer. II. Identification of the tryptophan residues acting as energy donors. *J. Biol. Chem.* **273**, 33198–33202 (1998).
60. Guan, L., Smirnova, I. N., Verner, G., Nagamori, S. & Kaback, H. R. Manipulating phospholipids for crystallization of a membrane transport protein. *Proc. Natl Acad. Sci. USA* **103**, 1723–1726 (2006).
61. Otwinowski, Z. & Minor, W. in *Methods in Enzymology, Part A, Macromolecular Crystallography*, Vol. 276, 307–326 (Academic Press, 1997).
62. Winn, M. D. *et al.* Overview of the CCP4 suite and current developments. *Acta Crystallogr. D Biol. Crystallogr.* **67**, 235–242 (2011).
63. Adams, P. D. *et al.* PHENIX: a comprehensive Python-based system for macromolecular structure solution. *Acta Crystallogr. D Biol. Crystallogr.* **66**, 213–221 (2010).
64. Padilla, J. E. & Yeates, T. O. A statistic for local intensity differences: robustness to anisotropy and pseudo-centering and utility for detecting twinning. *Acta Crystallogr. D Biol. Crystallogr.* **59**, 1124–1130 (2003).
65. Zhang, Y. I-TASSER server for protein 3D structure prediction. *BMC Bioinformatics* **9**, 40 (2008).
66. McCoy, A. J. *et al.* Phaser crystallographic software. *J. Appl. Crystallogr.* **40**, 658–674 (2007).
67. Lee, S., Sawaya, M. R. & Eisenberg, D. Structure of superoxide dismutase from *Pyrobaculum aerophilum* presents a challenging case in molecular replacement with multiple molecules, pseudo-symmetry and twinning. *Acta Crystallogr. D Biol. Crystallogr.* **59**, 2191–2199 (2003).
68. Emsley, P., Lohkamp, B., Scott, W. G. & Cowtan, K. Features and development of Coot. *Acta Crystallogr. D Biol. Crystallogr.* **66**, 486–501 (2010).
69. Baker, N. A., Sept, D., Joseph, S., Holst, M. J. & McCammon, J. A. Electrostatics of nanosystems: application to microtubules and the ribosome. *Proc. Natl Acad. Sci. USA* **98**, 10037–10041 (2001).
70. Schroedinger, L. *The PyMOL Molecular Graphics System*. Version 1.5 (2013).

Acknowledgements

We thank Luis Reuss and R. Bryan Sutton for critical reading of the manuscript, and Shailika Nurva, Hariharan Parameswaran, Elena Tikhonova, Gill Verner and Shushi Nagamori for assistance. We thank Kelsey Markham for constructing most of the mutants. We also thank the staffs at the Advanced Light Source, Lawrence Berkeley National Laboratory and the Stanford Synchrotron Radiation Light Source for assistance with X-ray data collection. The diffraction data set was collected at ALS BL 5.0.2. This work was supported by the National Science Foundation (grant MCB-1158085 to L.G. and grant MCB-0450970 to H.R.K.) and the Norman Hackerman Advanced Research Program (grant 010674-0034-2009 to L.G.), as well as by the National Institutes of Health (grants R21HL087895 and R01GM095538 to L.G. and grants R01DK051131 and R01DK069463 to H.R.K.).

Author contributions

A.S.E., M.S.Y. and L.G. performed protein production, crystallization, X-ray diffraction, data collection and processing. A.S.E. and L.G. performed collection and processing of data for the PDB accession 4M64 and structure interpretation. L.G., A.S.E. and A.A. designed and A.A. performed all transport assays and FRET measurements. L.G. interpreted functional data and directed the research. H.R.K. and G.L. provided advice and research reagents. All authors contributed to manuscript preparation. L.G. and A.S.E. wrote the manuscript with help from H.R.K.

Additional information

Accession codes: The protein coordinates and structure factor have been deposited in the Protein Data Bank with the accession number 4M64.

Supplementary Information accompanies this paper at <http://www.nature.com/naturecommunications>

Competing financial interests: The authors declare no competing financial interests.

Reprints and permission information is available online at <http://npg.nature.com/reprintsandpermissions/>

How to cite this article: Ethayathulla, A. S. *et al.* Structure-based mechanism for Na⁺/melibiose symport by MelB. *Nat. Commun.* 5:3009 doi: 10.1038/ncomms4009 (2014).



This work is licensed under a Creative Commons Attribution-NonCommercial-ShareAlike 3.0 Unported License. To view a copy of this license, visit <http://creativecommons.org/licenses/by-nc-sa/3.0/>